Hydrodynamics of Writing with Ink

Jungchul Kim,[1] Myoung-Woon Moon,[2] Kwang-Ryeol Lee,[2] L. Mahadevan,[3] and Ho-Young Kim[1,*]

[1]School of Mechanical and Aerospace Engineering, Seoul National University, Seoul 151-744, Korea
[2]Interdisciplinary and Fusion Technology Division, KIST, Seoul 136-791, Korea
[3]School of Engineering and Applied Sciences, Department of Physics, Harvard University, Cambridge, Massachusetts 02138, USA

(Received 3 May 2011; published 20 December 2011)

Writing with ink involves the supply of liquid from a pen onto a porous hydrophilic solid surface, paper. The resulting linewidth depends on the pen speed and the physicochemical properties of the ink and paper. Here we quantify the dynamics of this process using a combination of experiment and theory. Our experiments are carried out using a minimal pen, a long narrow tube that serves as a reservoir of liquid, which can write on a model of paper, a hydrophilic micropillar array. A minimal theory for the rate of wicking or spreading of the liquid is given by balancing the capillary force that drives the liquid flow and the resistance associated with flow through the porous substrate. This allows us to predict the shape of the front and the width of the line laid out by the pen, with results that are corroborated by our experiments.

DOI: 10.1103/PhysRevLett.107.264501 PACS numbers: 47.55.nb, 47.56.+r, 68.03.Cd, 68.08.Bc

For millenia, writing has been the preferred way to convey information and knowledge from one generation to another. We first developed the ability to write on clay tablets with a point, and then settled on a reed pen, as preserved from 3000 BC in Egypt when it was used with papyrus [1]. This device consisted of a hollow straw that served as an ink reservoir and allowed ink to flow to its tip by capillary action. A quill pen using a similar mechanism served as the instrument of choice for scholars in medieval times, while modern times have seen the evolution of variants of these early writing instruments to a nib pen, a ballpoint pen, and a roller ball pen. However, the fundamental action of the pen, to deliver liquid ink to an absorbent surface, has remained unchanged for five thousand years.

Although capillary imbibition on porous substrates has been studied for decades [2–6], how liquids spread on a rough substrate (paper) from a moving source (pen), a basic process underlying ink writing, seems to not have been treated thus far. Writing with a given pen leaves a marked trail whose character is determined by the ink, the paper, and the speed and style with which one moves the pen, and an example is shown in Fig. 1. To understand the characteristic hydrodynamics of this process, we employ a minimal system consisting of a straight capillary tube, our pen, that is held close to a hydrophilic micropillar array, our porous paper (see Fig. 2), and moves parallel to it. The shape and size of the liquid trail that results is what we call writing, and arises as a consequence the quasi-two-dimensional hydrodynamic problem of capillary-induced spreading from a moving source.

The model pen is an open glass capillary tube (inner radius $R \in [0.25\ 1.00]$ mm, wall thickness 0.1 mm) filled with a liquid that is translated by a linear stage at a speed u_0, which varies in the range [0–3.0] mm/s while maintained constant in each experiment. The inner surface of the tube is cleaned with a piranha solution to have a nearly zero contact angle with all the liquids used here, while the outer surface is coated with PTFE (polytetrafluoroethylene), which is hydrophobic, to prevent the liquid from climbing onto the outside. Our model inks were aqueous glycerine solutions with different concentrations: 63 (liquid A), 73 (B) and 78.5 (C) wt % and ethylene glycol 99 wt % (D), whose physical properties are listed in supplemental material [7]. The model paper was a silicon wafer decorated with cylindrical micropillar arrays which are formed by the DRIE (deep reactive ion etching) process, and then additionally plasma-etched by O_2 to make them superhydrophilic [8]. The individual pillars are cylindrical [Fig. 2(b)] with height h and diameter d, and arranged in a square array with pitch s: $\{h, d, s\} \in [10–20]$ μm. The liquid from the tube starts to wick into the forest of pillars as the tube bottom gently touches the substrate, and a CCD (charge coupled device) camera (frame rate 30 s^{-1}) is used to image the spreading front.

Placing a pen on paper before knowing what to write leads to a spreading stain that all of us have had some experience with. To understand the dynamics of the formation of this blot, we hold the pen fixed, and see a circular front emanating from it, as shown in Figs. 1(a) and 2(a). On these scales, fluid inertia is unimportant (Reynolds number based on the pillar height $\in [10^{-4} - 10^{-7}]$). The flow is driven by capillary forces at the spreading rim at a distance r from the source. The change in the surface energy associated with the increase of the blot size of radius from r to $r + dr$ is given by: $dE = 2\pi r[\gamma(1 - \frac{\pi}{4}d^2/s^2) + (f - \frac{\pi}{4}d^2/s^2)(\gamma_{SL} - \gamma_{SG})]dr = -2\pi\gamma(f - 1)rdr$, where γ, γ_{SL} and γ_{SG} is the interfacial tension between liquid-gas, solid-liquid and solid-gas, respectively, and f is the roughness defined as the ratio of the actual solid surface area to

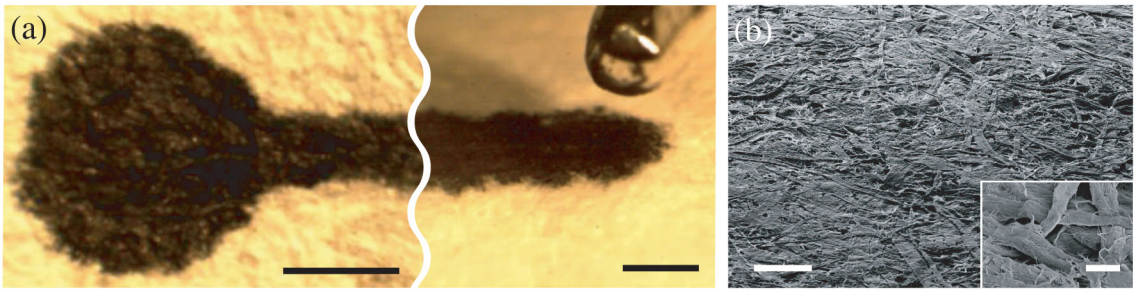

FIG. 1 (color online). Images of ink trail and paper. (a) A blot (generated by holding the pen at a fixed position for about 2 s, top view) and the end of the line (tilted view) that is drawn with a modern fountain pen on rice paper. Scale bars, 1 mm. (b) Scanning electron microscopy (SEM) images of rice paper surface. Scale bar in the main panel and the inset, 150 μm and 10 μm, respectively.

the projected area. Here we used Young's equation, $\gamma\cos\psi = \gamma_{SG} - \gamma_{SL}$, where the contact angle $\psi \approx 0$. The presence of a precursor film of the aqueous solutions on the superhydrophilic surface may change the absolute energy scales, but the energy change associated with replacing solid-gas interface by solid-liquid interface and that with covering the precursor liquid are the same, so that the analysis that follows remains qualitatively similar. In terms of the energy change, the driving force $F_{d,s} = -dE/dr = 2\pi\gamma(f-1)r$. Balancing this with the resisting force due to viscous shear stress which scales as $F_{r,s} \sim \mu U(r^2 - R^2)f/h$ (see [7]) gives $U = dr/dt \sim \phi\gamma rh/[\mu(r^2 - R^2)]$, where $\phi = (f-1)/f$. Here we have neglected the frictional resistance inside the tube and the effects of evaporation [7]. Integrating the preceding equation for U yields $\hat{r}^2 - \ln\hat{r}^2 - 1 \sim \tau$, where $\hat{r} = r/R$ and $\tau = 2\phi\gamma ht/(\mu R^2)$. For narrow tubes and late times, corresponding to $r^2 \gg R^2$, this result simplifies to yield [7]

$$r \sim \left(\phi\frac{\gamma}{\mu}h\right)^{1/2} t^{1/2}. \quad (1)$$

We thus see that an ink blot emerging from a pen spreads onto a stationary superhydrophilic surface with diffusive dynamics [9], where in addition to the classically known prefactor [10], $(\gamma h/\mu)^{1/2}$, the spreading rate depends on $\phi(f)$, the surface roughness. On real paper, the blot spreading is eventually limited by both contact line pinning at surface heterogenieties and evaporation. The spreading radii measured for different liquids and substrates collapse onto a single line with a slope of 0.51, consistent with our scaling law (1) [Fig. 2(c)].

We note that the spreading rate of an ink blot from a tube is different from the spreading of a drop on micropatterned surfaces. In the latter case, a fringe film diffusively extends beneath the bulk of the drop in a similar manner to (1), but the collapse of the bulk dominates the initial stages leading to a drop footprint that grows like $t^{1/4}$ [11]. This is also qualitatively different from the spreading of a drop on smooth surfaces where the radius grows like $t^{1/10}$ [12]. In contrast, the ink blot from a tube spreads rapidly and diffusively on rough surfaces ($f > 1$, $\phi > 0$), while it does not spread on smooth surfaces ($f = 1$, $\phi = 0$).

As shown in Fig. 3, a hydrophilic pen develops a capillary suction pressure $\Delta p_t = p_0 - p_t = 2\gamma/R - \rho gH$, where g is the gravitational acceleration and H is the liquid column height smaller than the equilibrium capillary rise height $2l_c^2/R$ with the capillary length $l_c = (\gamma/\rho g)^{1/2}$, which competes with the driving pressure $\Delta p_d = p_0 - p_e$ for spreading. Here p_0, p_t, and p_e are the pressure beneath the tube, at the top of the liquid column in the tube, and at the outer edge of the blot, respectively. For a blot

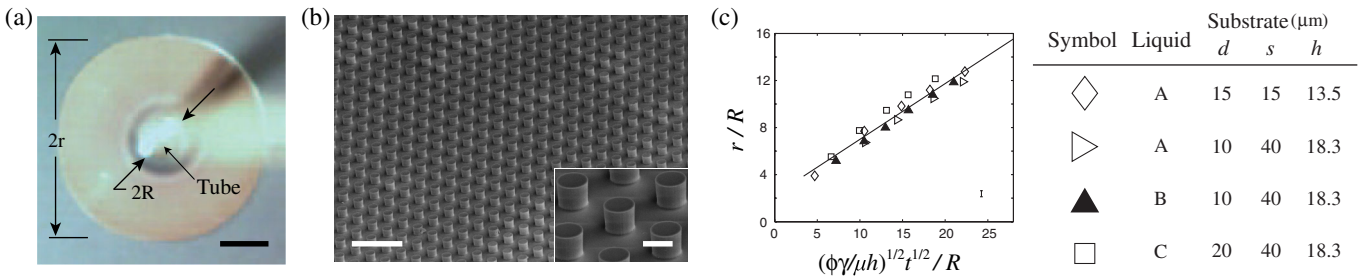

Symbol	Liquid	Substrate (μm) d	s	h
◇	A	15	15	13.5
▷	A	10	40	18.3
▲	B	10	40	18.3
□	C	20	40	18.3

FIG. 2 (color online). Blot formation on supherhydrophilic surfaces. (a) Top view of a liquid film emerging from a tube (which is out of focus) on a superhydrophilic surface. Scale bar, 1 mm. (b) SEM images of the superhydrophilic micropillar array. Scale bar in the main panel and the inset, 80 μm and 15 μm, respectively. (c) The scaled blot radius (r/R) plotted according to the scaling law (1). The slope of the best fitting straight line is 0.51, and the corresponding root mean square of deviation (RMSD) is 0.59. A characteristic error bar is shown in the lower right corner.

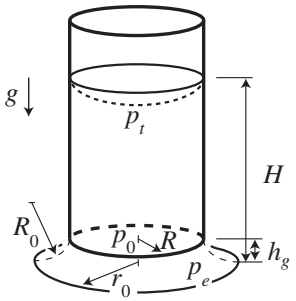

FIG. 3. Schematic of a small blot emitting from a tube on a smooth surface which is limited by the competition of the capillary suction pressure inside the tube and the Laplace pressure at the outer rim of the blot.

to spread beyond R on a rough surface, we must have $\Delta p_d \approx F_{d,s}|_{r=R}/(2\pi Rh) > \Delta p_t$, which yields a threshold roughness $f_{\min} \approx 1 + 2h/R - Hh/l_c^2 \in (1.04\text{–}1.07)$ for our experimental conditions. On a smooth substrate, the maximum radius of a blot r_0 is determined by the condition $\Delta p_t = \Delta p_d$, where $\Delta p_d = \gamma(R_0^{-1} - r_0^{-1})$ with R_0 being the radius of curvature of a meniscus between the substrate and the tube end that are separated by h_g; we find that $r_0/R \in (1.05\text{–}1.5)$ for $h_g/R \in (0 - 0.1)$ and $RH/l_c^2 \in (1 - 2)$.

Next, we consider the shape and width of the liquid film left behind by the pen which moves on the substrate with a constant velocity u_0, Fig. 4(a). We consider the coordinate system in Fig. 4(b), centered at the pen tip, with the wetting ink front denoted by a curve $r(\theta, t)$ that intersects an arbitrary but fixed vertical line AB at a point P with vertical coordinate w. We see then the radial velocity of the liquid front relative to the substrate is $\tilde{U} = \dot{w}\sin\theta$. Balancing the driving force of spreading in radial direction $\gamma(f - 1)r\Delta\theta$ with the resisting force $\mu\tilde{U}(r^2 - R^2)\Delta\theta f/h$ yields the expression $\tilde{U} \sim \phi\gamma h/(\mu r)$. Using the geometrical relations $\sin\theta = w/r$ and $\dot{w} = \dot{L}dw/dL$ with $\dot{L} = u_0$ finally allows us to determine the shape of the liquid front:

$$w \sim \eta(hL)^{1/2}, \tag{2}$$

where $\eta = (\phi/\mathrm{Ca})^{1/2}$ with the capillary number $\mathrm{Ca} = \mu u_0/\gamma$. Figure 4(c) shows the dimensionless liquid front profiles, w/R as a function of $\eta(hL)^{1/2}/R$, for different liquids and substrates; the data collapse on to a straight line with a slope 0.42. It is useful to point out that the parabolic front profile (2) is different from that of the Rankine half body constructed by superposing a radially axisymmetric fluid source with a uniform flow. This is because the source strength is not axisymmetric in our case; the flow from the pen is governed by the front profile which is a function of θ [7]. Furthermore, the relative motion between pen and substrate only drags along fluid at the interface: the rest of the fluid does not move at the same velocity owing to viscous shear.

Far from the parabolic front ahead of the pen, the ink front eventually stops moving and leaves behind an ink trail of finite width. This happens when the liquid has filled the gaps of the forest of micropillars and contact line pinning at the boundary of the wet array prevents further motion [7]. To determine the line width w_f, we consider the volume of liquid that wets the shaded area shown in Fig. 5(a) in a time $\Delta\tau$, given by $\Delta\Omega = 2w_f u_0 h\Delta\tau$. This is the sum of the amount of liquid that spreads outward on the surface, $\Delta\Omega_1$, and the volume of liquid that comes in direct contact with the substrate beneath the tube, $\Delta\Omega_2$, with $\Delta\Omega_1 \sim r\tilde{U}h\Delta\tau$, where $r\tilde{U} \sim \phi h\gamma/\mu$, and $\Delta\Omega_2 = 2Ru_0 h\Delta\tau$. Letting $\Delta\Omega = \Delta\Omega_1 + \Delta\Omega_2$, we find

$$\frac{w_f}{R} = \alpha\frac{\eta^2 h}{R} + \beta. \tag{3}$$

Figure 5(b) shows that the experimentally measured line thickness scaled by R is indeed linearly proportional to $\eta^2 h/R$ with $\alpha = 0.16$, and $\beta = 5.55$.

Having quantified the dynamics of spreading of a simple liquid onto a periodically structured micropillar array, we turn to the mechanics of writing on paper, which is

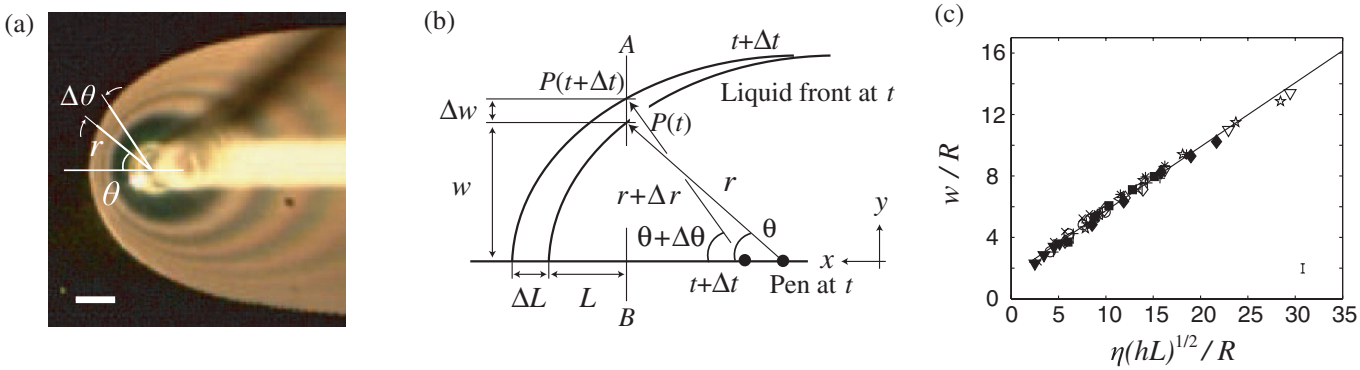

FIG. 4 (color online). Lines drawn by a moving pen. (a) A snapshot of the liquid film spreading on a substrate as it flows from a moving pen. Scale bar, 1 mm. (b) The coordinate system to describe the shape of the liquid front. (c) The scaled film profile (w/L) plotted according to the scaling law (2). The slope of the best fitting straight line is 0.42 with RMSD = 0.16. The experimental conditions for each symbol are listed in [7]. A characteristic error bar is shown.

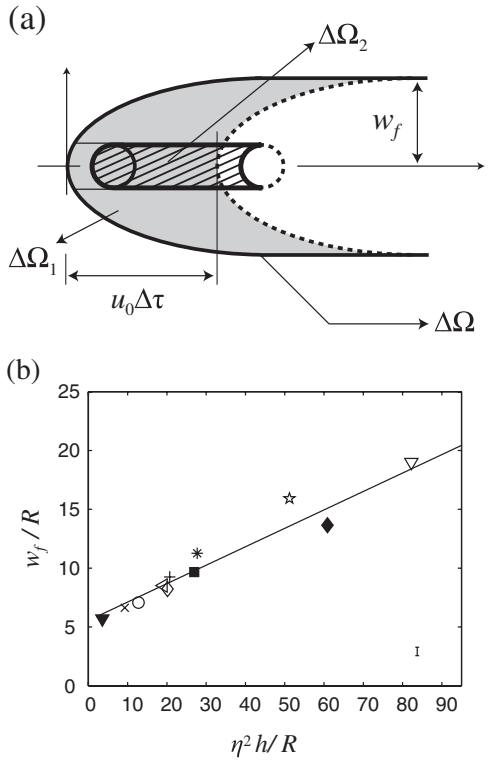

FIG. 5. (a) The shaded area wet by ink for a duration $\Delta\tau$, equals to $2w_f u_0 \Delta\tau$. (b) The dimensionless line thickness w_f/R scales linearly with $\eta^2 h/R$ regardless of liquid, pen speed, tube radius, and pillar array dimensions. The slope of the best fitting straight line is 0.16 and its extension meets the y axis at 5.55 with RMSD = 0.95. The experimental conditions for each symbol are listed in [7]. A characteristic error bar is shown.

isotropic in plane but has strong variations in pore structure and tortuosity through the thickness. A minimal modification of our theory to account for these effects would require us to modify the roughness factor f and make it a function of vertical depth and orientation, or equivalently modifying $\phi(\theta, z)$ to account for anisotropy and inhomogeneity of real paper. However, the approximate isotropy of the ink blot on paper shown in Fig. 1(a) suggests that this may not be necessary. To compare our scaling law and the size of the ink blot and line on real paper as shown in Fig. 1, we estimate the liquid film thickness (or pore size) $h \approx 5\ \mu$m and $\phi \approx 0.2$ based on the SEM image. The nib opening $2R = 0.1$ mm, and the ink has the surface tension $\gamma = 0.063$ N/m and viscosity $\mu \approx 3.8$ mPa · s [13]. When the pen is held stationary for ~2 s, the radius of the blot is predicted to follow $r = 0.51(\phi\gamma ht/\mu)^{1/2} + 1.71R \approx 3.0$ mm while when the pen is moving with a velocity $u_0 \approx 5$ mm/s the line width is predicted to follow $w_f = 0.16\eta^2 h + 5.55R \approx 0.82$ mm, estimates which compare reasonably with the actual radius 1.3 mm and the width 0.7 mm. However, we note that the theory overestimates the blot radius more than it does for the line width, which is probably due to paper swelling.

Our experiments and scaling laws capture the basic hydrodynamics of ink writing associated with the spreading of a Newtonian liquid on a porous substrate. Real inks are not Newtonian and furthermore dry quickly; in addition modern pens are more sophisticated than the simple quill nibs of yore. In ballpoint pens, for example, the linewidth is set by the dimension of the ball and its mode of contact with paper, as a relatively viscous shear thinning ink that dries very quickly is spread out by a rolling ball. Understanding how to combine the dynamics of swelling and imbibition in soft porous media with the rate of deposition will allow us to create functional porous substrates by writing on ever smaller scales—perhaps even rejuvenating the ink-pen in a different guise?

This work was supported by National Research Foundation of Korea (Grant Nos. 2009-0076168 and 412-J03001), KIST, SNU-IAMD (H.-Y. K.), and the MacArthur Foundation (L. M.).

*hyk@snu.ac.kr

[1] S. R. Fischer, *A History of Writing* (Reaktion, London, 2005).
[2] E. W. Washburn, Phys. Rev. **17**, 273 (1921).
[3] S. H. Davis and L. M. Hocking, Phys. Fluids **12**, 1646 (2000).
[4] C. Ishino, M. Reyssat, E. Reyssat, K. Okumura, and D. Quéré, Europhys. Lett. **79**, 56 005 (2007).
[5] L. Courbin, E. Denieul, E. Dressaire, M. Roper, A. Ajdari, and H. A. Stone, Nature Mater. **6**, 661 (2007).
[6] M. Conrath, N. Fries, M. Zhang, and M. E. Dreyer, Transp. Porous Media **84**, 109 (2010).
[7] See Supplemental Material at http://link.aps.org/supplemental/10.1103/PhysRevLett.107.264501 for detailed theories and experimental conditions.
[8] J. W. Yi, M.-W. Moon, S. F. Ahmed, H. Kim, T.-G. Cha, H.-Y. Kim, S.-S. Kim, and K.-R. Lee, Langmuir **26**, 17 203 (2010).
[9] A. Marmur, J. Colloid Interface Sci. **124**, 301 (1988).
[10] P.-G. de Gennes, F. Brochard-Wyart, and D. Quéré, *Capillarity and Wetting Phenomena* (Springer, New York, 2004).
[11] S. J. Kim, M.-W. Moon, K.-R. Lee, D.-Y. Lee, Y. S. Chang, and H.-Y. Kim, J. Fluid Mech. **680**, 477 (2011).
[12] L. H. Tanner, J. Phys. D **12**, 1473 (1979).
[13] Our measurement with a rheometer indicates that the ink shows a slightly shear-thickening behavior, that is, the viscosity increases with the shear rate. In our experiments, the shear rate is approximately (5 mm/s)/(5 μm) = 100 s^{-1}, and the corresponding viscosity is 3.8 mPa · s.

Supplemental Material for "Hydrodynamics of writing with ink"

1. Liquid properties at 23°C

	Liquid	Concentration (wt%)	γ (N/m)	μ (Pa·s)
A	Glycerine	63	0.0659	0.0136
B	Glycerine	73	0.0651	0.0306
C	Glycerine	78.5	0.0648	0.0488
D	Ethylene Glycol	99	0.0484	0.0209

2. Viscous resistance due to micropillar arrays

Observing the side view of the liquid spreading through a forest of micropillars, we found that the tops of the pillars are barely wetted during the initial propagation of the wet front. The top surfaces get wet only after the gaps between the pillars are filled with liquid, thus the dominant contribution to the dissipation is associates with liquid flow between the pillars. Then the shear force exerted by the side of the pillars $F_{r,1} \sim \mu U(f-1)(r^2-R^2)/d_s$, where $d_s = (s - \frac{\pi}{4}d)/2$ is half the average distance between the adjacent pillars. The shear force exerted by the base $F_{r,2} \sim \mu U(1-f_t)(r^2-R^2)/h$, so that the total resisting force $F_{r,s} = F_{r,1}+F_{r,2} \sim \mu U(r^2-R^2)(f/h+c)$. We note that $c/(f/h)$ is typically smaller than 0.1 in our experimental conditions, thus we may write $F_{r,s} \sim \mu U(r^2-R^2)f/h$. Here we have neglected the Oseen-type resistance around a cylindrical pillar $F_o \sim O(h)$. For $h < s$, $F_{r,s} \sim h^{-1}$ dominates $F_o \sim h$ [4], consistent with our measurements.

3. Neglecting resistance in the tube

As liquid flows from the tube onto a hydrophilic surface, there is viscous resistance from both the interior wall of the tube as well as the substrate. The resistance from the tube wall $F_{r,t} \sim 2\pi\mu R h_t U_t/R$, where U_t is the flow speed inside the tube and h_t is the liquid column height in the tube, with U_t related to U via volume conservation via the relation $\pi R^2 \mathrm{d}h_t = 2\pi r h(1-f)\mathrm{d}r$, so that $U_t = 2rh(1-f_t)U/R^2$. Because the resistance from the substrate $F_{r,s} \sim \mu U r^2 f/h$ for $r^2 \gg R^2$, the ratio $F_{r,t}/F_{r,s} \sim 4h^2 h_t(1-f)/(R^2 r f) \leq 0.05$ for the substrates and the pens used in

our study. Therefore, the friction from the tube wall can be neglected in evaluating the resisting force of the liquid flow.

4. Simplification leading to equation (1)

We rearrange the relation $U = \mathrm{d}r/\mathrm{d}t \sim \phi\gamma r h/[\mu(r^2 - R^2)]$ to find that

$$\int_R^r \frac{r^2 - R^2}{r}\mathrm{d}r \sim \int_0^t \frac{\phi\gamma h}{\mu}\mathrm{d}t$$

Taking the coefficient of proportionality to be unity and integrating, we get

$$\left(\frac{r}{R}\right)^2 - \ln\left(\frac{r}{R}\right)^2 - 1 = \tau \tag{S1}$$

where the dimensionless time $\tau = 2\phi\gamma h t/(\mu R^2)$. Figure S1 compares this result with that obtained by using the approximation $(r^2 - R^2)/r \approx r$, which yields the simple result

$$\frac{r}{R} = \tau^{1/2}$$

We see that the the error associated with approximating $(r^2 - R^2)/r \approx r$ becomes negligible as τ increases, when the front radius is much larger than the pen radius. For example, when $r/R = 10$, the relative error is less than 3%.

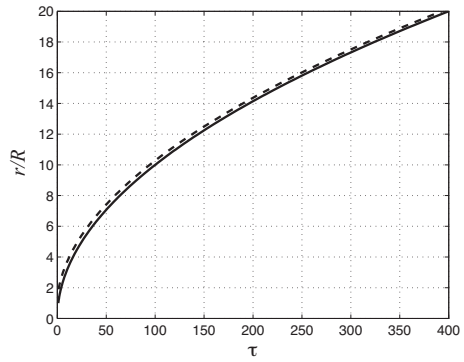

Figure S1: Comparison of the radial evolution models of a blot with (broken line) and without (solid line) including the tube radius R.

5. Effects of evaporation

As the area wetted by the liquid from the pen increases, evaporation can limit spreading of the liquid. This effect acts over and above that associated with contact line pinning due to surface

heterogenieties. Here we estimate the radius of a liquid blot, r_e, at which the evaporative loss of the liquid (over the entire blot area) becomes comparable to the liquid flux supplied by the tube. The evaporative mass flux of water vapor per unit area $J \sim D\Delta c/\delta$, where D and c, respectively, are the diffusivity and the concentration of vapor, and $\delta(r)$ is the boundary layer thickness of the vapor concentration at distance r from the center of the pen, given by $\delta \sim \sqrt{D(t-\tau)}$, where t and τ are the time taken for the liquid film to extend by r_e and r, respectively, from the time when the pen contacts the substrate. Using the relation $U(r) \sim \phi\gamma h/(\mu r)$ that follows from Eq. (1) in the text, we find that $t \sim \mu r_e^2/(\phi\gamma h)$ and $\tau \sim \mu r^2/(\phi\gamma h)$. Balancing the mass flux from the tube and the evaporative flux leads to $\rho U r_e h \sim \int Jr\mathrm{d}r$ where ρ is the density of the liquid. Substituting our earlier expressions for the various functions into this conservation equation yields an estimate for the maximum radius of the wetted region

$$r_e \sim \frac{\rho}{\Delta c}\left(\frac{\gamma\phi h^3}{\mu D}\right)^{1/2}$$

Adopting typical transport properties of water vapor $D \approx 2.6 \times 10^{-5}$ m^2/s and $\Delta c \approx 7 \times 10^{-3}$ kg/m^3 [F.P. Incropera et al. *Fundamentals of Heat and Mass Transfer*, 6th ed. (2007)] leads to the estimate $r_e \sim 0.1 - 1$ m for water, which is much greater than typical size of the writing. Assuming that the evaporation properties of glycerine do not differ much from those of water, this justifies our neglect of the effects of evaporation in the dynamics of liquid spreading considered here. However, for real inks that are formulated to allow quick drying, D can be much greater than that of water so that it is possible that r_e is reduced substantially in such situations.

6. Comparison of the front profile drawn by the moving pen and the superposition of a diffusive source and a constant advection

The Rankine half body is constructed by the superposition of a point source and a uniform stream [G.K. Batchelor, *An Introduction to Fluid Dynamics* (1967) p. 461]. When we superpose a point source producing a radial flow of magnitude $v_r = m/(2r)$, where m corresponds to the source strength, and a uniform flow u_0 in the horizontal direction, the stagnation streamline is given by $y = m(\pi - \theta)/(2\pi u_0)$. To see whether this matches the observed liquid front profile drawn by a moving pen, we consider two different source strengths: (i) that of the stationary pen with $m \approx 0.13\phi\gamma h/\mu$, the empirical constant obtained to try and best fit Fig. 2c, and (ii) that used to match the final line thickness w_f, $m = 2u_0 w_f$. Fig. S2(a) shows that the superposition

of an axisymmetric source with a uniform stream predicts the line shapes (I and II) that are quite different from the actually observed front profile. Indeed, even when we arbitrarily adjusted the location of the sources to match the stagnation point with the experiments, Fig. S2(b), the difference persists.

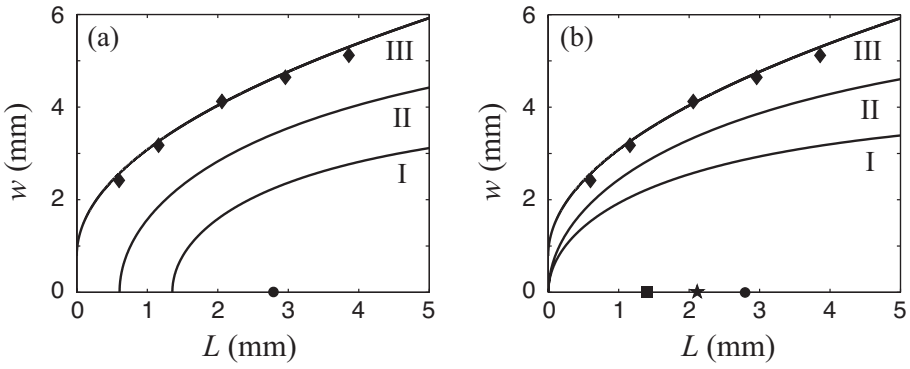

Figure S2: Comparison of the Rankine-half bodies and the actual front profile of the line (liquid B) drawn by a pen of $R = 0.5$ mm moving with $u_0 = 0.3$ mm on the substrate with $[h, d, s] = [18.3, 10, 40]$ μm. Lines I and II are the predictions of the Rankine half body model which match the source strength of the stationary pen and the final line width, respectively. Line III is the parabolic profile of this work with the empirical parameters obtained via Fig. 4(c). Diamonds correspond to experimental measurements. (a) The locations of the actual pen and the sources of the Rankine half body model coincide. (b) The source locations (a square for line I and a star for line II) have been adjusted to match the stagnation point at the origin. The filled circles in (a) and (b) correspond to the location of the pen.

7. Symbols in Figs. 4c and 5b.

Symbol	Liquid	u_0 (mm/s)	R (mm)	Substrate (μm) d	s	h	f
◁	A	2.5	0.5	15	30	13.5	1.71
■	B	0.8	0.5	15	30	13.5	1.71
◆	B	0.3	0.5	10	40	18.3	1.36
×	C	1.3	0.5	15	30	13.5	1.71
○	C	0.8	0.5	10	40	18.3	1.36
◇	C	0.8	0.5	20	40	18.3	1.72
▼	C	0.8	0.5	10	40	9.0	1.18
▽	D	0.8	0.25	15	30	13.5	1.71
✳	D	0.8	0.4	15	30	13.5	1.71
☆	D	0.8	0.75	15	30	13.5	1.71
+	D	0.8	0.1	15	30	13.5	1.71

Figure S3: Experimental conditions for the symbols in Figs. 4c and 5b.

8. The mechanism defining the line width.

Fig. S4 shows the (a) experimental image and (b) schematic side view of the edge of the liquid film laid out by a moving pen which is bounded by the outermost pillars of the wet area. The meniscus pinned at the pillars of the boundary of wet area must overcome the energy barrier associated with contact line pinning in order to advance to the next row, which is unlikely due to the absence of liquid supply. Although the free energy of the system can be lowered to an extent by wetting another row, the pinning effect appears to dominate over this free energy reduction process as experimentally observed. Ref. [5], which investigated the spreading of a liquid drop on hydrophilic micropillar array, also observed that the drop volume controls the size of the wetted area (Fig. 4c therein).

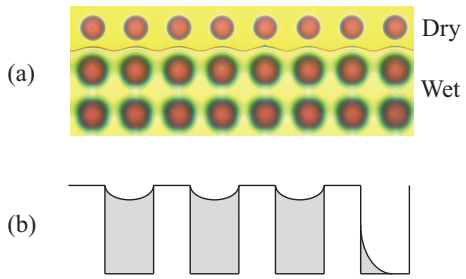

Figure S4: (a) Top view of the edge of the film of liquid C on the micropillar array with $[h, d, s] = [13.5, 15, 30]$ μm. (b) Schematic of the side view of the edge of the liquid film.